Published in final edited form as:
Proteins. 2008 May 1; 71(2): 525–533. doi:10.1002/prot.21828.

The 1.38 Å crystal structure of DmsD protein from *Salmonella typhimurium*, a proofreading chaperone on the Tat pathway

Yang Qiu[1], **Rongguang Zhang**[2], **T. Andrew Binkowski**[2], **Valentina Tereshko**[1], **Andrzej Joachimiak**[1,2], and **Anthony Kossiakoff**[1,*]

1*Department of Biochemistry and Molecular Biology, The University of Chicago, Chicago, Illinois 60637*

2*Argonne National Laboratory, Biosciences Division, Structural Biology Center and Midwest Center for Structural Genomics, Argonne, Illinois 60439*

Abstract

The DmsD protein is necessary for the biogenesis of dimethyl sulphoxide (DMSO) reductase in many prokaryotes. It performs a critical chaperone function initiated through its binding to the twin-arginine signal peptide of DmsA, the catalytic subunit of DMSO reductase. Upon binding to DmsD, DmsA is translocated to the periplasm via the so-called twin-arginine translocation (Tat) pathway. Here we report the 1.38 Å crystal structure of the protein DmsD from Salmonella typhimurium and compare it with a close functional homolog, TorD. DmsD has an all-α fold structure with a notable helical extension located at its N-terminus with two solvent exposed hydrophobic residues. A major difference between DmsD and TorD is that TorD structure is a domain-swapped dimer, while DmsD exists as a monomer. Nevertheless, these two proteins have a number of common features suggesting they function by using similar mechanisms. A possible signal peptide-binding site is proposed based on structural similarities. Computational analysis was used to identify a potential GTP binding pocket on similar surfaces of DmsD and TorD structures.

Keywords

DmsD; *proofreading chaperone*; *DmsA*; *DMSO reductase*; *Tat protein translocation pathway*

INTRODUCTION

DMSO reductase is a membrane-anchored respiratory enzyme that is essential for many prokaryotes to grow anaerobically on DMSO and many related S- and N-oxides, such as trimethylamine N-oxide (TMAO).[1-7] The enzyme is composed of a molybdo-bis (molybdoperin guanine dinucleotide) cofactor-containing catalytic subunit (DmsA), a four [4Fe-4S]-cluster containing electron-transfer subunit (DmsB), and a hydrophobic, membrane spanning anchor subunit (DmsC). DmsA is transported across the cytoplasmic membrane in a fully-folded, cofactor-loaded state through a protein translocation system termed the twin-

Correspondence to: Andrzej Joachimiak.

*Correspondence to: Anthony Kossiakoff, Department of Biochemistry and Molecular Biology, The University of Chicago, 929 E. 57th St., Chicago, Illinois 60637. E-mail: E-mail: koss@bsd.uchicago.edu or Andrzej Joachimiak, Argonne National Laboratory, Biosciences Division, Structural Biology Center and Midwest Center for Structural Genomics, 9700 South Cass Avenue, Building 202, Argonne, Illinois 60439. E-mail: E-mail: andrzejj@anl.gov.

arginine translocase (Tat) pathway,[8,9] which has been discovered recently in the cytoplasmic membrane of many prokaryotes and the thylakoid membranes of plant chloroplasts.[10-12]

Proteins transported by the Tat system contain a characteristic twin-arginine motif SRRXFLK in their signal peptide.[8] DmsA and TMAO reductase (TorA), represent a subset of exo-cytoplasmic respiratory enzymes with redox-active cofactors and have been shown to use the Tat pathway.[8,9] They both belong to the DMSO reductase family and share a similar overall structure containing four domains and a molybdenum cofactor, but they differ in their first domain sequences.[13-20] This difference influences their substrate specificities with DmsA reducing a wide range of S- and N-oxide compounds, whereas TorA specifically reduces TMAO.[21,22]

The Tat pathway is an independent and complementary translocation system to the well-characterized Sec pathway for protein secretion,[23-26] and has the unique ability to transport fully-folded and oligomerized proteins across cytoplasmic membranes.[25,26] Its core structure comprises three membrane-associated proteins, TatA, TatB, and TatC.[27-29] The TatBC unit is the twin-arginine signal peptide recognition module,[29] whereas TatA forms a large oligomeric ring-structure purported to be the protein-conducting channel.[30,31] It is thought that Tat substrates initially bind to the TatBC module in a energy-independent step,[32-34] subsequently the channel module (TatA) associates with the TatBC-substrate complex in a step powered solely by the transmembrane proton gradient and ultimately facilitates transport of the substrate proteins.[34,35]

Prior to the periplasmic translocation via the Tat pathway, Tat substrates are subject to a chaperone-mediated screen termed “Tat proofreading” that prevents the translocation of immature proteins before cofactor-loading, correct folding, or docking of partner proteins have occurred.[36] It has been established that DmsD and TorD are involved, respectively, in the biogenesis of DMSO reductase and TMAO reductase by acting as “Tat proofreading” chaperones.[37-42]

Since DmsD and TorD have relatively low sequence identity (~20%) but have similar functions, a structural comparison of the proteins provides insights into the structural basis for their functions. The crystal structure of TorD from *Shewanella massilia* (Sm-TorD in the following text) was reported recently and showed an unusual domain swapped homodimer structure distinct from all the protein structures in PDB.[43] Here we present the crystal structure of DmsD from *S. typhimurium* (St-DmsD in this study) at 1.38 Å resolution. Unlike TorD, St-DmsD is a monomer in the crystal. It has an all-α fold and is similar to one of the subunits of the dimeric TorD structure. Comparison of these two structures reveals some conserved structural features supporting functional similarities. Additionally, based on the GTP-binding property of TorD demonstrated by Hatzixanthis *et al.*,[44] we identified a potential GTP binding site adjacent to the protruding N-terminal helices on similar surfaces of the St-DmsD and Sm-TorD structures by modeling analysis.

MATERIALS AND METHODS

Protein expression and purification

The gene was cloned into the pMCSG7 vector to generate an expression clone producing a fusion protein with an N-terminal His-6-tag and a TEV protease recognition site (ENLYFQ↓S). A selenomethionine (Se-Met) derivative of the St-DmsD was prepared as described previously[45] and purified according to standard protocol.[46] The transformed BL21 cells were grown in M9 medium at 37°C. M9 medium was supplied with 0.4% sucrose, 8.5 m*M* NaCl, 0.1 m*M* $CaCl_2$, 2 m*M* $MgSO_4$, and 0.001%$_0$ thiamine. After OD_{600} reached 0.5, 0.005% (w/v) of each of leucine, isoleusine, lysine, phenylalanine, threonine, and valine were added to

inhibit the metabolic pathway of methionine and encourage Se-Met incorporation. Se-Met was then added at 0.006% (w/v) and 15 min later protein expression was induced by 1 m*M* isopropyl-β-D-thiogalactoside (IPTG). The cells were then grown at 20°C overnight.

The harvested cells were resuspended in lysis buffer (500 m*M* NaCl, 5% glycerol, 50 m*M* HEPES, pH 8.0, 10 m*M* imidazole, 10 m*M* 2-mercaptoethanol). About 1 mg/mL lysozyme and 100 μL of a protease inhibitor cocktail (Sigma, P8849) were added per 2 g of wet cells, and the cells were kept on ice for 20 min before sonication. The lysate was clarified by centrifugation at $27{,}000_g$ for 1 h and then applied to a 5-mL HiTrap Ni-NTA column (Amersham Biosciences) on the AKTA EXPLORER 3D (Amersham Biosciences). The His_6-tagged protein was eluted using elution buffer (500 m*M* NaCl, 5% glycerol, 50 m*M* HEPES, pH 8.0, 250 m*M* imidazole, 10 m*M* 2-mercaptoethanol), and the His_6 tag was cleaved from the protein by treatment with recombinant His-tagged TEV protease (a gift from Dr. D. Waugh, NCI). A second Ni-NTA affinity chromatography was performed manually to remove the His-tag and His-tagged TEV protease. The protein was dialyzed against 20 m*M* HEPES (pH 8.0), 150 m*M* NaCl, and 1 m*M* DTT, then concentrated using centrifugal concentrators and stored at liquid nitrogen temperature.

Crystallization and data collection

The protein was crystallized by vapor diffusion in sitting drops containing 0.5 μL of protein solution (15 mg/mL) and 0.5 μL of reservoir solution (20% PEG400, 1*M* ammonium sulfate, 10% glycerol, pH 8.0 imidazole). Mixed solutions were equilibrated at 20°C against the reservoir solution. Crystals appeared on day two and grew to the size about 0.4 × 0.2 × 0.1 mm^3 in 1 week. A single crystal was picked up from the solution and frozen in liquid nitrogen. The absorption edge of Se was determined by X-ray fluorescence scan of the crystal, followed by examination of the fluorescence data using CHOOCH.[47] A two-wavelength MAD data set was collected at 100 K with 2 s/1°/frame using a ADSC Q315 detector and a 120 mm crystal-to-detector distance at the Structural Biology Center 19ID beamline of the Advanced Photon Source, Argonne National Laboratory. Data were processed and scaled using HKL2000 suite[48] and are summarized in Table I.

Structure solution and refinement

The phases were determined using SOLVE[49] with two wavelength MAD data and the three selenium sites gave a figure of merit 0.47 and Z score 14.9. The initial model was built automatically by RESOLVE[50] with 92% of total residues placed, and then improved manually using the TURBO-FRODO[51,52] program. The final electron density map was well connected except for the residues 117-122, which are disordered in the crystal structure. Water molecules were assigned using ARP/wARP[53] and the structure was refined using REFMAC5.[54] The final *R* factor was 0.16 and *R* free was 0.19 (Table II). Atomic coordinates and structure factors have been deposited into the PDB with ID 1S9U.

Surface analysis

Protein surfaces were compared by local sequence composition, local shape, and local orientation between residues located on geometrically defined pockets or voids by the pvSOAR search algorithm. pvSOAR is based on the methodology described in Binkowski *et al.*[55] and is used here to identify similar surface regions in three dimensional protein structures. Searches were conducted by comparing all surfaces of St-DmsD and TorD to the Global Protein Surface Survey (http://gpss.mcsg.anl.gov) library of annotated surface patterns. The query surfaces were searched against all GTP binding surfaces. Statistically significant search results were then manually inspected for biological relevance and modeled into the structures of St-DmsD and TorD.

RESULTS

The crystal structure of the St-DmsD protein has been solved using MAD phasing and refined to 1.38 Å. The crystals belong to the space group C2 with cell dimensions of a = 85.40 Å, b = 79.36 Å, c = 43.47 Å, α = γ = 90°, β = 115.1°. There is one 204-residue molecule in the asymmetric unit with a Matthews coefficient of 2.5 and the solvent content ~50%. There are four selenium sites in the St-DmsD protein sequence (four Met residues); however, only three (including the N-terminal one) can be located from the anomalous data. The fourth Met is located within the disordered loop region (117-122) and could not be positioned by either the anomalous Patterson map or the anomalous difference Fourier map. The MAD data are summarized in Table I and the refinement statistics and the model geometry statistics are given in Table II.

Overall structure

The overall structure of St-DmsD is a compact all α-helical fold consisting of 12 α-helices [Fig. 1(A)]. Size exclusion chromatography shows the protein is a monomer in solution (data not shown). Residues 117-122 form an extended loop and are disordered in the structure [Fig. 1 (A)]. A notable feature of the structure is the N-terminal α-helical extension (residues 1-8) that protrudes ~10 Å out of the globular structure [Fig. 1(A)]. Besides the N-terminal Met, this helix contains two other hydrophobic residues (Phe4 and Leu5) that are exposed to the solvent in the monomer [Fig. 1(B)], but become buried in the crystal by contacting with a two-fold symmetry related molecule. It is possible that the unusual hydrophobic helical extension may provide the potential membrane accessibility *in vivo*, because DmsD can be associated with the inner membrane of *Escherichia coli* and interacts with the TatBC subunits on the membrane.[39]

Sequence analysis and structural comparisons

A PSI_BLAST search against the nonredundant Gen-Bank revealed that, with the *E*-value below 1×10^{-5}, St-DmsD has over 430 sequence homologues distributed mainly in bacteria (>95%) with a few members in archaea and viruses. Many of these homologues are annotated as "hypothetical" proteins, while some of them are designated as the cytoplasmic chaperones TorD and DmsD. Although sequence comparisons reveal that St-DmsD does not share high sequence identity with TorD proteins, it does share high sequence identity (>64%) with other DmsD proteins from *E. coli*, *Salmonella paratyphi-a*, and *Shigella flexnerii*. Sequences of nine homologues are aligned in Figure 2 using ClustalW. The sequence motif E(Q)PXDHXG(A) XXL is found in both TorD and DmsD protein homologs and residues D126 and H127 have been confirmed by mutagenesis to play an important role in the TorD function.[36,41,44]

TorD from *Shewanella masilia* (Sm-TorD)[43] is a distant sequence homolog of St-DmsD sharing 21% sequence identity and 41% sequence similarity. Sm-TorD is a dimer characterized by an extensive domain swapping of four C-terminal α-helices. These helices are parts of a tightly packed core unit in St-DmsD [H9-H12 shown on Fig. 1(A)]. Each spatially separated subunit of the Sm-TorD homodimer can be superposed well with the monomeric St-DmsD structure with a Z score of 13.6 and an RMSD of 3 Å over 159 Cα atom pairs [Fig. 3(A)]. Schematic representations of the domain relationships of Sm-TorD and St-DmsD are shown in Figure 3(B).

Although St-DmsD and Sm-TorD are in different oligomeric forms, they share some notable common features. First, they both have a long loop/hinge region (residues 113-127 in St-DmsD; residues 121-135 in Sm-TorD) separating the N- and C-terminal domains of the proteins. Secondly, they have an α-helical extension protruding out the globular structure (N-terminal H1 in St-DmsD and C-terminal extension, residues 202-210 in Sm-TorD). Consequently, the

hydrophobic residues on the protruding helices are virtually solvent-exposed in the solution (Phe4 and Leu5 on St-DmsD, and Val205, Ile207, and Ile208 on Sm-TorD). Finally, the nine identical residues together with 12 highly conserved residues identified in the sequence alignment (see Fig. 2) are also structurally conserved between St-DmsD and Sm-TorD structures. They contribute largely to a prominent concave surface and are distributed similarly with respect to the protruding helical extensions. [Fig. 3(C)].

There are several differences in the structures of St-DmsD and Sm-TorD, which likely reflect different constraints due to oligomeric state and insertions/deletions in sequences. Most notable is the orientation of the helix located before the long loop/hinge region [Fig. 3(A)].

The loop region of St-DmsD monomer and the hinge region that bridges the two globular domains of Sm-TorD dimer consist of 15 residues (see the green box in Fig. 2). Five of these residues are conserved across the DmsD-TorD proteins. The E(Q)PXDH sequence motif is conserved in all TorD family members.[41] Biochemical and mutagenesis experiments have demonstrated that the substitution of D124 and H125 in *E. coil* TorD with Ala abolishes Tat proofreading function.[36,41,44] Taken together, these data suggest the E(Q)PXDH sequence motif, together with other conservative residues spatially arranged around this motif, is a good candidate for the binding site of the signal peptide [Fig. 3(C)]. Both the loop of the St-DmsD (113-127) and the hinge of the Sm-TorD (121-135) are mainly hydrophilic and rich in negatively charged residues, which could potentially form an electrostatic environment to attract the positively charged N-terminal region of the twin-arginine signal peptide of the target protein and facilitate the docking of signal peptide into the putative binding site.

Identifying a putative GTP binding site

Hatzixanthis *et al.*[44] reported that TorD binds GTP with weak (about 370 μM) affinity and modeled a GTP-binding site based on the coordinates of a DTT molecule cocrystallized with Sm-TorD. To explore potential GTP binding pockets, we performed a surface analysis of the St-DmsD and Sm-TorD structures using the Global Protein Surface Survey server[55,56] (http://gpss.mcsg.anl.gov). Surfaces from each structure with solvent accessible surface area greater than 100 $Å^2$ (the minimum observed protein surface area of GTP binding pockets in structures deposited to the PDB) were compared with a library of 209 GTP binding sites using the pvSOAR algorithm, which identifies local sequence composition, shape and orientation between surface residues.[55]

Both structures had corresponding surfaces that showed significant similarity to a GTP binding surface from guanylyl cyclase from H. *sapiens* (PDB ID = 1awl) (see Fig. 4). A well-defined cavity with molecular surface area of 495 $Å^2$ and a volume of 964 $Å^3$ found on DmsD (CASTp ID = 22) shared 11 conserved residues [Fig. 4(A, B, E)] with the GTP binding surface of guanylyl cyclase from *H. sapiens*, which superimpose giving a cRMSD and oRMSD *P*-value of 8.84×10^{-3} and 7.20×10^{-8}. The site on the St-DmsD structure involves residues Glu148, Glu140, Phe10, Leu193, and Leu151, which are completely conserved across the DmsD family, but not necessarily across the TorD family (see Fig. 2). A GTP molecule has been modeled into this predicted pocket in St-DmsD structure based on the superposition of the conserved residues [Fig. 4(A,B)].

The conserved residues between the GTP binding surface from guanylyl cyclase and the Sm-TorD and St-DmsD structures are shown in Figure 4(E). The GTP binding site proposed here is different than that proposed by Hatzixanthis *et al.*,[44] but they share a conserved residue, Phe41. It has been shown that the F41A variant lost Tat proofreading activity by an *in vivo* assay using the *E. coil* TorD protein.[44] It is interesting to note that the potential GTP-binding sites of both St-DmsD and Sm-TorD are adjacent to the protruding terminal helices. Although the functional role of GTP-binding is unknown in the process of TorD/DmsD chaperoning,

their structural locations may suggest a supportive role in switching TorD/DmsD molecules between the attachment-detachment states of TatBC subunits by cooperation with the extended hydrophobic helical terminus.

DISCUSSION

The DmsD protein is a member of TorD family of molecular chaperones and is an essential factor for the survival of anaerobic bacteria on media containing DMSO.[40] DmsD functions as a chaperone of the catalytic subunit of membrane-anchored DMSO reductase, DmsA, which is transported into the periplasm through the Tat translocase machinery. DmsD binds to the signal peptide of DmsA facilitating the complete folding and incorporation of the cofactor and the transportation of DmsA across the inner membrane via the Tat pathway.[38,57,58]

The related chaperone, TorD, plays a similar role, but on a different substrate, TorA, a TMAO reductase. Although the crystal structure of Sm-TorD is a domain-swapped homodimer, dimerization is not implicated in its chaperone function.[44] The TorD monomer is fully capable of binding the signal peptide, performing Tat proofreading, and targeting the compatible enzyme to Tat translocation apparatus. A specific requirement for TorD oligomerization has not been reported for any of these steps.[44] It was reported that during Sm-TorD purification, the domain swapped dimeric Sm-TorD forms only a minor component, whereas the monomer is the major component.[43] The surface area buried between the N-terminal domain (H1-H8) and the C-terminal domain (H9-H12, a four-helix bundle) of monomeric St-DmsD structure is 2572 $Å^2$ and highly hydrophobic (~72% of hydrophobic atoms), indicating the hydrophobic interactions are the major force in stabilizing the monomer of St-DmsD. Likewise, the dimer interface in TorD (about 4500 $Å^2$ of surface area) is also predominantly hydrophobic with polar interactions playing a minor role in stabilizing the two globular units of the Sm-TorD dimer.[43] While there are a number of structures of domain-swapped proteins in the PDB and 3D domain swapping may represent a general mechanism for switching between two protein conformers,[59] it remains an open question whether the domain-swapped Sm-TorD dimer structure is the functional form of the protein.

The crystal structure of St-DmsD reported here reveals a monomeric structure for the TorD chaperone family. Comparison of St-DmsD and Sm-TorD structures identifies some shared conserved features in spite of their different oligomeric forms. First, there is an extended terminal helix with several hydrophobic residues exposed to the solvent (Phe4 and Leu5 on the N-terminal of St-DmsD structure; Val205, Ile207, and Ile208 on the C-terminal of Sm-TorD). We hypothesize that this feature is important in targeting substrates toward the membrane-anchored Tat system. Secondly, all the conserved residues shared by nine members of TorD family including St-DmsD and Sm-TorD are positioned and orientated similarly in these two structures [Fig. 3(C)]. Furthermore, the Asp-His motif conserved in all members of TorD family is located in a prominent long loop region found in both structures. Some of these conserved residues may contribute directly to the substrate binding, for example, the experimentally established Asp-His motif. On the basis of the results of GTP-binding property of TorD demonstrated by Hatzixanthis *et al.*[44] 1, a potential GTP binding site was modeled on the similar structural surfaces of St-DmsD and Sm-TorD. This site is adjacent to the protruding terminal helices, suggesting a supportive role in switching TorD/DmsD molecules between the attachment-detachment states of the TatBC subunits.

CONCLUSIONS

By comparison with the domain-swapped structure of TorD, our results reveal some significant features shared by the monomeric structure of DmsD. Although both proteins belong to the same superfamily and have been experimentally determined as the “Tat proofreading”

chaperones, DmsD and TorD act on distantly related twin-arginine leaders[60] and the twin-arginine leaders of DmsA and TorA are not completely interchangeable.[61] What determines the specificities of these two chaperones remains an open question. Ilbert *et al.*[41] have shown both *in vitro* and *in vivo* that in *E. coli*, TorA maturation specifically depends on *E. coli* TorD (Ec-TorD) and neither *E. coli* DmsD nor Sm-TorD could substitute for Ec-TorD. Further mutagenesis studies are needed to identify and characterize the key residues responsible for distinguishing different twin-arginine leaders. Structural characterization of a chaperone-signal peptide complex should reveal the detailed binding surface and may explain how the chaperone specifically binds to its target.

ACKNOWLEDGMENTS

We appreciate Dr. Aretha Fiebig for reviewing the manuscript. We wish to thank all members of the Structural Biology Center at Argonne National Laboratory for their help in conducting experiments.

Grant sponsor: National Institutes of Health; Grant numbers: GM62414, GM074942; Grant sponsor: U.S. Department of Energy, Office of Biological and Environmental Research; Grant number: W-31-109-Eng-38.

REFERENCES

1. Sagai M, Ishimoto M. An enzyme reducing adenosine 1N-oxide in *Escherichia coli*, amine N-oxide reductase. J Biochem (Tokyo) 1973;73:843–859. [PubMed: 4578389]
2. Bilous PT, Cole ST, Anderson WF, Weiner JH. Nucleotide sequence of the dmsABC operon encoding the anaerobic dimethylsulphoxide reductase of *Escherichia coli*. Mol Microbiol 1988;2:785–795. [PubMed: 3062312]
3. Weiner JH, MacIsaac DP, Bishop RE, Bilous PT. Purification and properties of *Escherichia coli* dimethyl sulfoxide reductase, an iron-sulfur molybdoenzyme with broad substrate specificity. J Bacteriol 1988;170:1505–1510. [PubMed: 3280546]
4. Silvestro A, Pommier J, Pascal MC, Giordano G. The inducible trimethylamine N-oxide reductase of *Escherichia coli* K12: its localization and inducers. Biochim Biophys Acta 1989;999:208–216. [PubMed: 2512991]
5. Yamamoto I, Hinakura M, Seki S, Seki Y, Kondo H. Reduction of N-oxide and S-oxide compounds by *Escherichia coli*. J Gen Appl Microbiol 1989;35:253–259.
6. Sambasivarao D, Scraba DG, Trieber C, Weiner JH. Organization of dimethyl sulfoxide reductase in the plasma membrane of *Escherichia coli*. J Bacteriol 1990;172:5938–5948. [PubMed: 2170332]
7. Sambasivarao D, Weiner JH. Differentiation of the multiple S- and N-oxide-reducing activities of *Escherichia coli*. Curr Microbiol 1991;23:105–110.
8. Berks BC. A common export pathway for proteins binding complex redox cofactors? Mol Microbiol 1996;22:393–404. [PubMed: 8939424]
9. Weiner JH, Bilous PT, Shaw GM, Lubitz SP, Frost L, Thomas GH, Cole JA, Turner RJ. A novel and ubiquitous system for membrane targeting and secretion of cofactor-containing proteins. Cell 1998;93:93–101. [PubMed: 9546395]
10. Dalbey RE, Kuhn A. Evolutionarily related insertion pathways of bacterial, mitochondrial, and thylakoid membrane proteins. Annu Rev Cell Dev Biol 2000;16:51–87. [PubMed: 11031230]
11. Robinson C, Bolhuis A. Protein targeting by the twin-arginine translocation pathway. Nat Rev Mol Cell Biol 2001;2:350–356. [PubMed: 11331909]
12. Yen MR, Tseng YH, Nguyen EH, Wu LF, Saier MH Jr. Sequence and phylogenetic analyses of the twin-arginine targeting (Tat) protein export system. Arch Microbiol 2002;177:441–450. [PubMed: 12029389]
13. Weiner JH, Rothery RA, Sambasivarao D, Trieber CA. Molecular analysis of dimethylsulfoxide reductase: a complex iron-sulfur molybdoenzyme of *Escherichia coli*. Biochim Biophys Acta 1992;1102:1–18. [PubMed: 1324728]
14. Simala-Grant JL, Weiner JH. Kinetic analysis and substrate specificity of *Escherichia coli* dimethyl sulfoxide reductase. Microbiology 1996;142:3231–3239. [PubMed: 8969520]

15. Hill R. The mononuclear molybdenum enzymes. Chem Rev 1996;96:2757–2816. [PubMed: 11848841]
16. Schindelin H, Kisker C, Hilton J, Rajagopalan KV, Rees DC. Crystal structure of DMSO reductase: redox-linked changes in molybdopterin coordination. Science 1996;272:1615–1621. [PubMed: 8658134]
17. McAlpine AS, McEwan AG, Bailey S. The high resolution crystal structure of DMSO reductase in complex with DMSO. J Mol Biol 1998;275:613–623. [PubMed: 9466935]
18. Czjzek M, Dos Santos JP, Pommier J, Giordano G, Mejean V, Haser R. Crystal structure of oxidized trimethylamine N-oxide reductase from *Shewanella massilia* at 2.5 A resolution. J Mol Biol 1998;284:435–447. [PubMed: 9813128]
19. Richardson DJ. Bacterial respiration: a flexible process for a changing environment. Microbiology 2000;146:551–571. [PubMed: 10746759]
20. McDevitt CA, Hugenholtz P, Hanson GR, McEwan AG. Molecular analysis of dimethyl sulphide dehydrogenase from *Rhodovulum sulfidophilum*: its place in the dimethyl sulphoxide reductase family of microbial molybdopterin-containing enzymes. Mol Microbiol 2002;44:1575–1587. [PubMed: 12067345]
21. Iobbi-Nivol C, Pommier J, Simala-Grant J, Mejean V, Giordano G. High substrate specificity and induction characteristics of trimethylamine-N-oxide reductase of *Escherichia coli*. Biochim Biophys Acta 1996;1294:77–82. [PubMed: 8639717]
22. Simala-Grant JL, Weiner JH. Modulation of the substrate specificity of *Escherichia coli* dimethylsulfoxide reductase. Eur J Biochem 1998;251:510–515. [PubMed: 9492325]
23. Santini CL, Ize B, Chanal A, Muller M, Giordano G, Wu LF. A novel sec-independent periplasmic protein translocation pathway in *Escherichia coli*. EMBO J 1998;17:101–112. [PubMed: 9427745]
24. Settles AM, Martienssen R. Old and new pathways of protein export in chloroplasts and bacteria. Trends Cell Biol 1998;8:494–501. [PubMed: 9861672]
25. Clark SA, Theg SM. A folded protein can be transported across the chloroplast envelope and thylakoid membranes. Mol Biol Cell 1997;8:923–934. [PubMed: 9168475]
26. DeLisa MP, Tullman D, Georgiou G. Folding quality control in the export of proteins by the bacterial twin-arginine translocation pathway. Proc Natl Acad Sci USA 2003;100:6115–6120. [PubMed: 12721369]
27. Berks BC, Sargent F, Palmer T. The Tat protein export pathway. Mol Microbiol 2000;35:260–274. [PubMed: 10652088]
28. Yahr TL, Wickner WT. Functional reconstitution of bacterial Tat translocation in vitro. EMBO J 2001;20:2472–2479. [PubMed: 11350936]
29. Alami M, Trescher D, Wu LF, Muller M. Separate analysis of twin-arginine translocation (Tat)-specific membrane binding and translocation in *Escherichia coli*. J Biol Chem 2002;277:20499–20503. [PubMed: 11923313]
30. Jack RL, Sargent F, Berks BC, Sawers G, Palmer T. Constitutive expression of *Escherichia coli* tat genes indicates an important role for the twin-arginine translocase during aerobic and anaerobic growth. J Bacteriol 2001;183:1801–1804. [PubMed: 11160116]
31. Sargent F, Gohlke U, De Leeuw E, Stanley NR, Palmer T, Saibil HR, Berks BC. Purified components of the *Escherichia coli* Tat protein transport system form a double-layered ring structure. Eur J Biochem 2001;268:3361–3367. [PubMed: 11422364]
32. Cline K, Mori H. Thylakoid DeltapH-dependent precursor proteins bind to a cpTatC-Hcf106 complex before Tha4-dependent transport. J Cell Biol 2001;154:719–729. [PubMed: 11502764]
33. de Leeuw E, Granjon T, Porcelli I, Alami M, Carr SB, Muller M, Sargent F, Palmer T, Berks BC. Oligomeric properties and signal peptide binding by *Escherichia coli* Tat protein transport complexes. J Mol Biol 2002;322:1135–1146. [PubMed: 12367533]
34. Alami M, Luke I, Deitermann S, Eisner G, Koch HG, Brunner J, Muller M. Differential interactions between a twin-arginine signal peptide and its translocase in *Escherichia coli*. Mol Cell 2003;12:937–946. [PubMed: 14580344]
35. Mori H, Cline K. A twin arginine signal peptide and the pH gradient trigger reversible assembly of the thylakoid [Delta]pH/Tat translocase. J Cell Biol 2002;157:205–210. [PubMed: 11956224]

36. Jack RL, Buchanan G, Dubini A, Hatzixanthis K, Palmer T, Sargent F. Coordinating assembly and export of complex bacterial proteins. EMBO J 2004;23:3962–3972. [PubMed: 15385959]
37. Pommier J, Mejean V, Giordano G, Iobbi-Nivol C. TorD, a cytoplasmic chaperone that interacts with the unfolded trimethylamine N-oxide reductase enzyme (TorA) in *Escherichia coli*. J Biol Chem 1998;273:16615–16620. [PubMed: 9632735]
38. Oresnik IJ, Ladner CL, Turner RJ. Identification of a twin-arginine leader-binding protein. Mol Microbiol 2001;40:323–331. [PubMed: 11309116]
39. Papish AL, Ladner CL, Turner RJ. The twin-arginine leader-binding protein. Dms D, interacts with the Tat B and Tat C subunits of the *Escherichia coli* twin-arginine translocase. J Biol Chem 2003;278:32501–32506. [PubMed: 12813051]
40. Ray N, Oates J, Turner RJ, Robinson C. DmsD is required for the biogenesis of DMSO reductase in *Escherichia coli* but not for the interaction of the DmsA signal peptide with the Tat apparatus. FEBS Lett 2003;534:156–160. [PubMed: 12527378]
41. Ilbert M, Mejean V, Iobbi-Nivol C. Functional and structural analysis of members of the TorD family, a large chaperone family dedicated to molybdoproteins. Microbiology 2004;150:935–943. [PubMed: 15073303]
42. Berks BC, Palmer T, Sargent F. Protein targeting by the bacterial twin-arginine translocation (Tat) pathway. Curr Opin Microbiol 2005;8:174–181. [PubMed: 15802249]
43. Tranier S, Iobbi-Nivol C, Birck C, Ilbert M, Mortier-Barriere I, Mejean V, Samama JP. A novel protein fold and extreme domain swapping in the dimeric TorD chaperone from *Shewanella massilia*. Structure 2003;11:165–174. [PubMed: 12575936]
44. Hatzixanthis K, Clarke TA, Oubrie A, Richardson DJ, Turner RJ, Sargent F. Signal peptide-chaperone interactions on the twin-arginine protein transport pathway. Proc Natl Acad Sci USA 2005;102:8460–8465. [PubMed: 15941830]
45. Walsh MA, Dementieva I, Evans G, Sanishvili R, Joachimiak A. Taking MAD to the extreme: ultrafast protein structure determination. Acta Crystallogr D Biol Crystallogr 1999;55:1168–1173. [PubMed: 10329779]
46. Kim Y, Dementieva I, Zhou M, Wu R, Lezondra L, Quartey P, Joachimiak G, Korolev O, Li H, Joachimiak A. Automation of protein purification for structural genomics. J Struct Funct Genomics 2004;5:111–118. [PubMed: 15263850]
47. Evans G, Pettifer RF. CHOOCH: a program for deriving anomalous-scattering factors from X-ray fluorescence spectra. J Appl Cryst 2001;34:82–86.
48. Otwinowski Z, Minor W. Processing of X-ray diffraction data collected in oscillation mode. Methods Enzymol 1997;276:307–326.
49. Terwilliger TC, Berendzen J. Automated MAD and MIR structure solution. Acta Crystallogr D Biol Crystallogr 1999;55:849–861. [PubMed: 10089316]
50. Terwilliger TC. Automated main-chain model building by template matching and iterative fragment extension. Acta Crystallogr D Biol Crystallogr 2003;59:38–44. [PubMed: 12499537]
51. Jones TA. A graphics model building and refinement system for macromolecules. Appl Cryst 1978;11:268–272.
52. Roussel, A.; Cambillau, C. Silicon graphics directory. Silicon Graphics; Mountain View, CA: 1991. Turbo Frodo.
53. Lamzin VS, Wilson KS. Automated refinement for protein crystal-lography. Methods Enzymol 1997;277:269–305. [PubMed: 18488314]
54. Murshudov GN, Vagin AA, Dodson EJ. Refinement of macromolecular structures by the maximum-likelihood method. Acta Crystallogr D Biol Crystallogr 1997;53:240–255. [PubMed: 15299926]
55. Binkowski TA, Adamian L, Liang J. Inferring functional relationships of proteins from local sequence and spatial surface patterns. J Mol Biol 2003;332:505–526. [PubMed: 12948498]
56. Binkowski TA, Naghibzadeh S, Liang J. CASTp: Computed atlas of surface topography of proteins. Nucleic Acids Res 2003;31:3352–3355. [PubMed: 12824325]
57. Sargent F, Berks BC, Palmer T. Assembly of membrane-bound respiratory complexes by the Tat protein-transport system. Arch Microbiol 2002;178:77–84. [PubMed: 12115052]

58. Palmer T, Berks BC. Moving folded proteins across the bacterial cell membrane. Microbiology 2003;149:547–556. [PubMed: 12634324]

59. Liu Y, Eisenberg D. 3D domain swapping: as domains continue to swap. Protein Sci 2002;11:1285–1299. [PubMed: 12021428]

60. Voordouw G. A universal system for the transport of redox proteins: early roots and latest developments. Biophys Chem 2000;86:131–140. [PubMed: 11026678]

61. Sambasivarao D, Turner RJ, Simala-Grant JL, Shaw G, Hu J, Weiner JH. Multiple roles for the twin arginine leader sequence of dimethyl sulfoxide reductase of *Escherichia coli*. J Biol Chem 2000;275:22526–22531. [PubMed: 10801884]

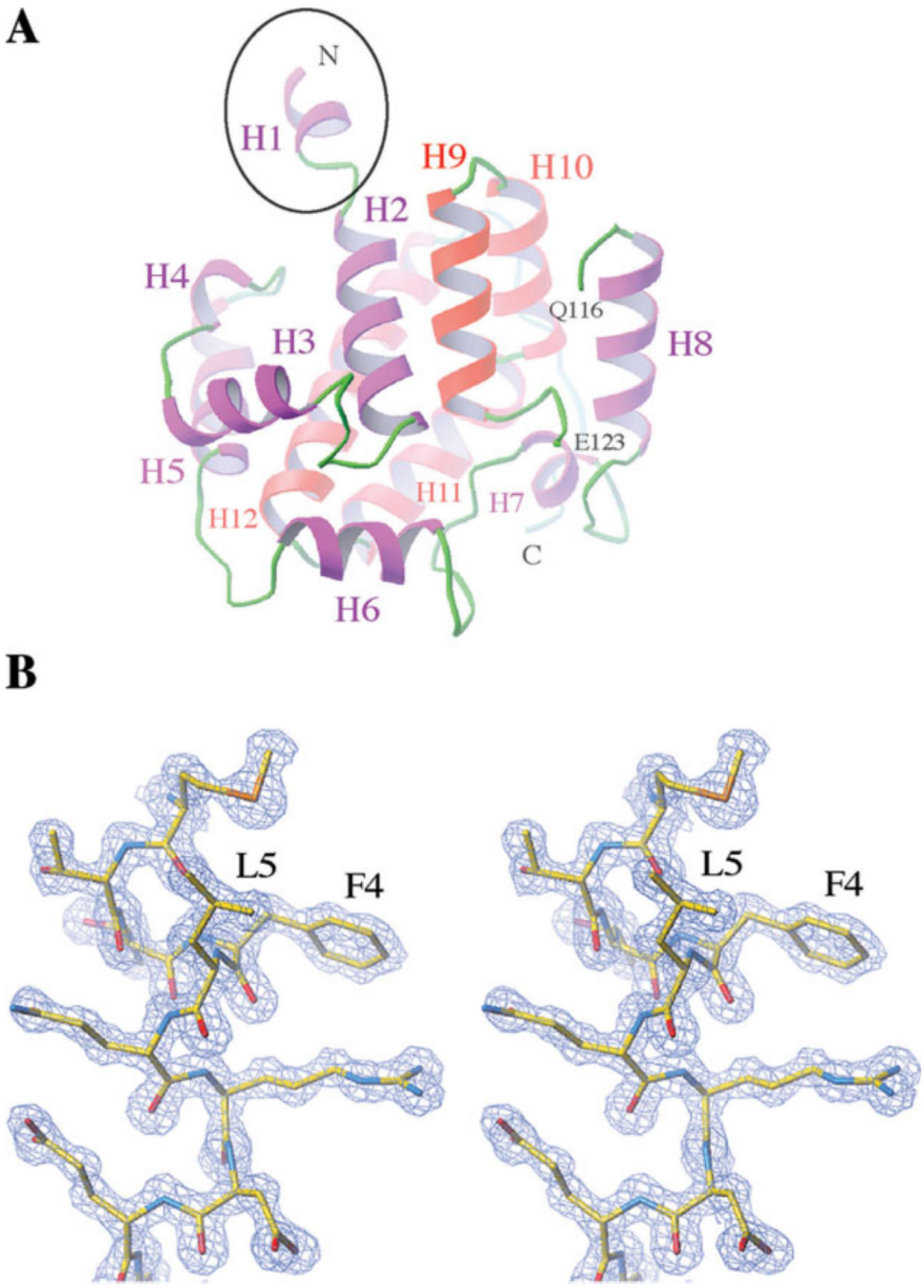

Figure 1.

(**A**) The all-alpha fold structure of DmsD from the S. typhimurium L12. The N-terminal extension is indicated by a black circle. The chain is broken at residues Q116 and E123 due to the missing residues. Helices from 1 to 12 are labeled. (**B**) Stereo view of the electron densities around the N-terminal extension (residues 1-8) at 1σ level. Residues are shown by stick representations.

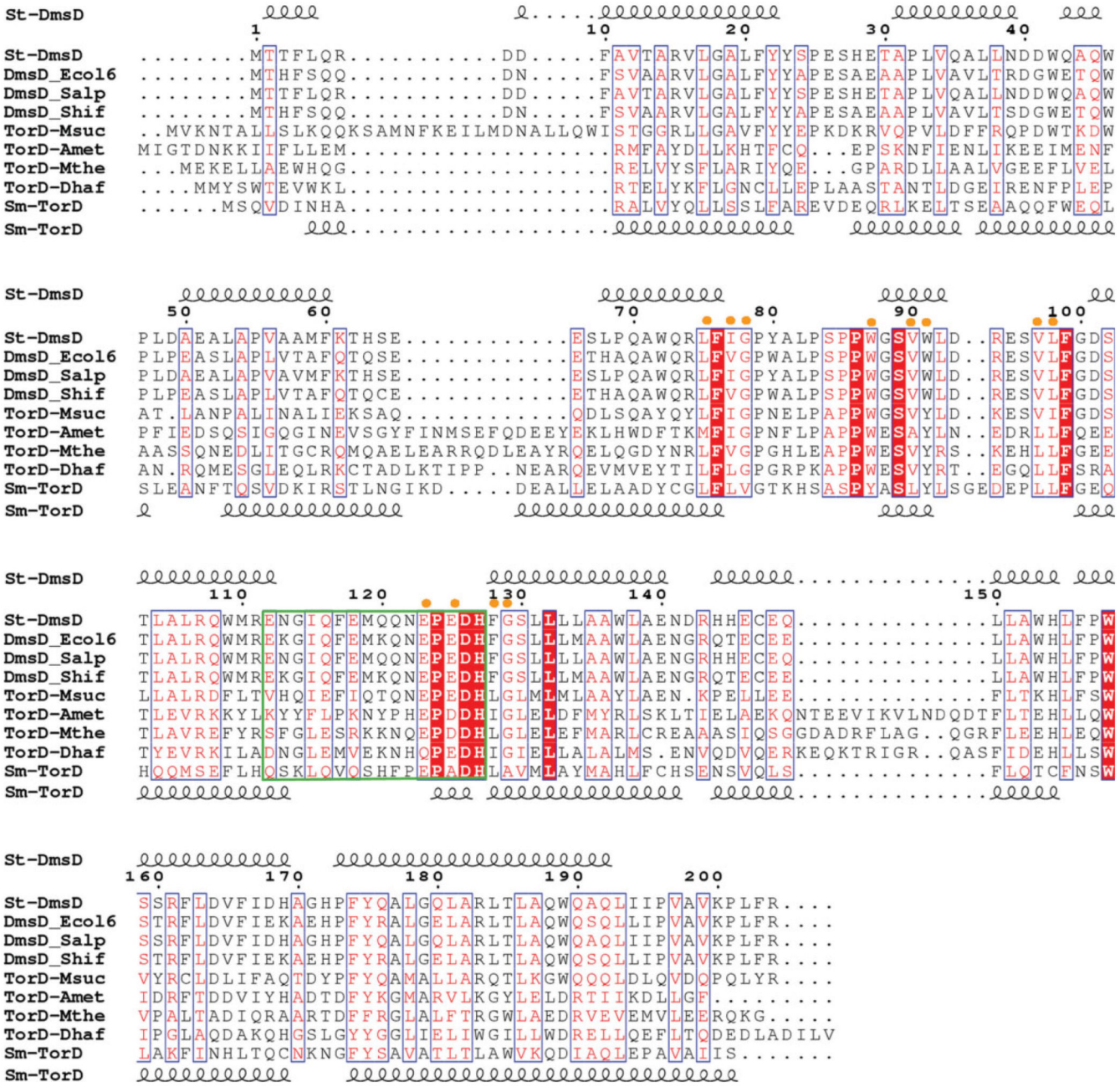

Figure 2.

ClustalW alignment of St-DmsD and TorD homologues (gi|67460417| from S. typhimurium, gi|67460400| from E. coli, gi|67460198| from S. paratyphi, gi|67476814| from S. flexneri, gi|52426390| from M. succiniciproducens, gi|77684993| from A. metalliredigenes, gi |83590226| from M. thermoacetica, gi|68206032| from D. hafniense, gi|47117367| TorD from S. massilia). The E-value is below 1×10^{-5}. The secondary structure of St-DmsD is shown on the top and Sm-TorD on the bottom. The nine identical residues are highlighted in red, and the 12 highly conserved residues spatially close to the identical residues are indicated by yellow dots on top of the aligned sequences. The green box defines the flexible loop/hinge region between N-terminal and C-terminal moieties.

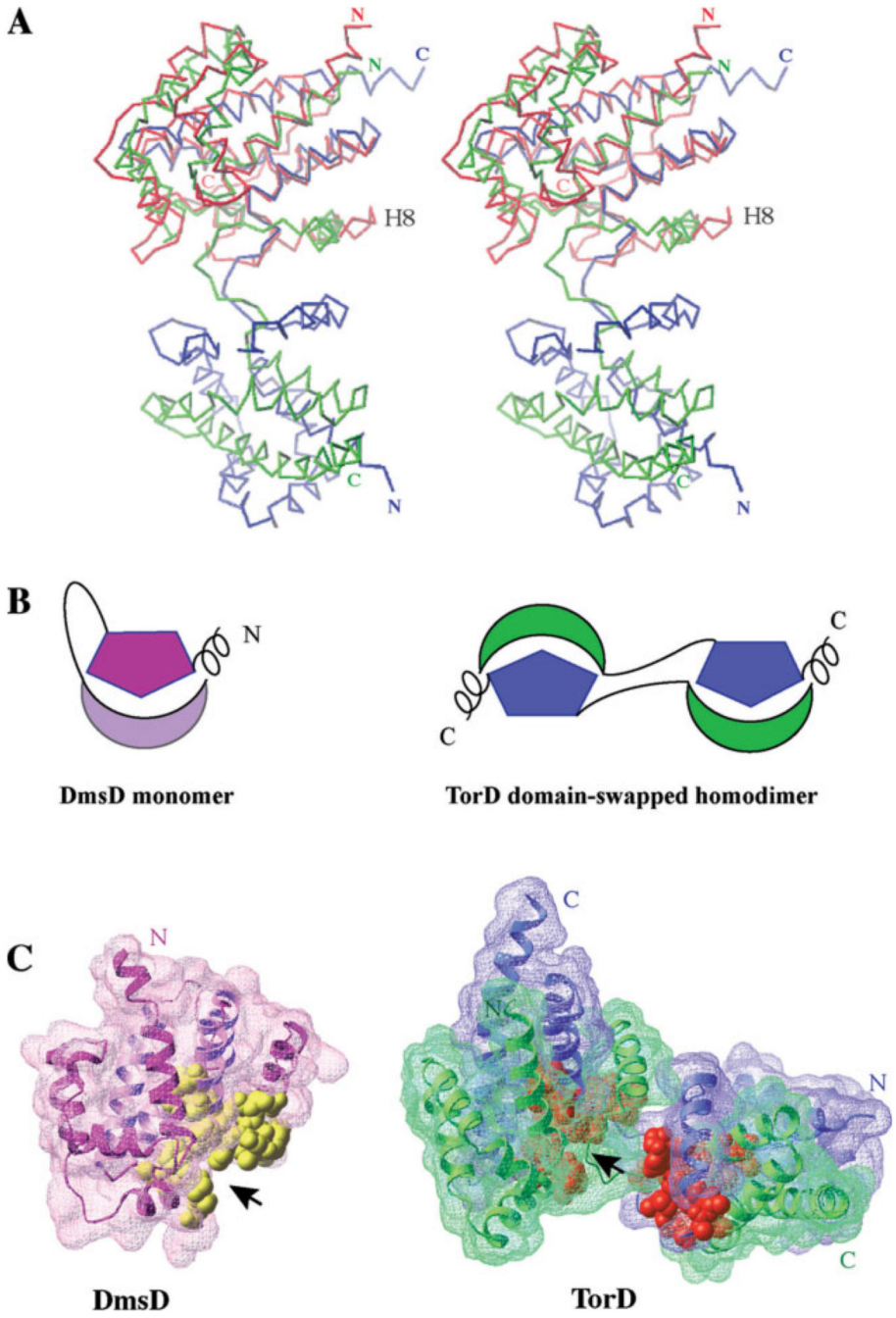

Figure 3.

(**A**) Stereo view of the DmsD structure (colored in red) superposed on one of the subunit of TorD homodimer. The two subunits of TorD are colored in blue and green. The most notable difference between the two structures is the orientation of the helix located before the long loop/hinge region, H8 in DmsD. (**B**) Cartoon representations of the DmsD monomer and the domain-swapped TorD homodimer. The helical extensions are located at the N-terminus of DmsD and the C-terminus of TorD. The hinge/loop regions between N-terminal moieties and C-terminal moieties are shown by lines. (**C**) Surface representations of DmsD monomer and TorD dimer with the conserved residues of TorD/DmsD family (see Fig. 2) displayed by CPK

representation in yellow (DmsD) and gold (TorD), respectively. The two chains of TorD homodimer are colored in blue and green.

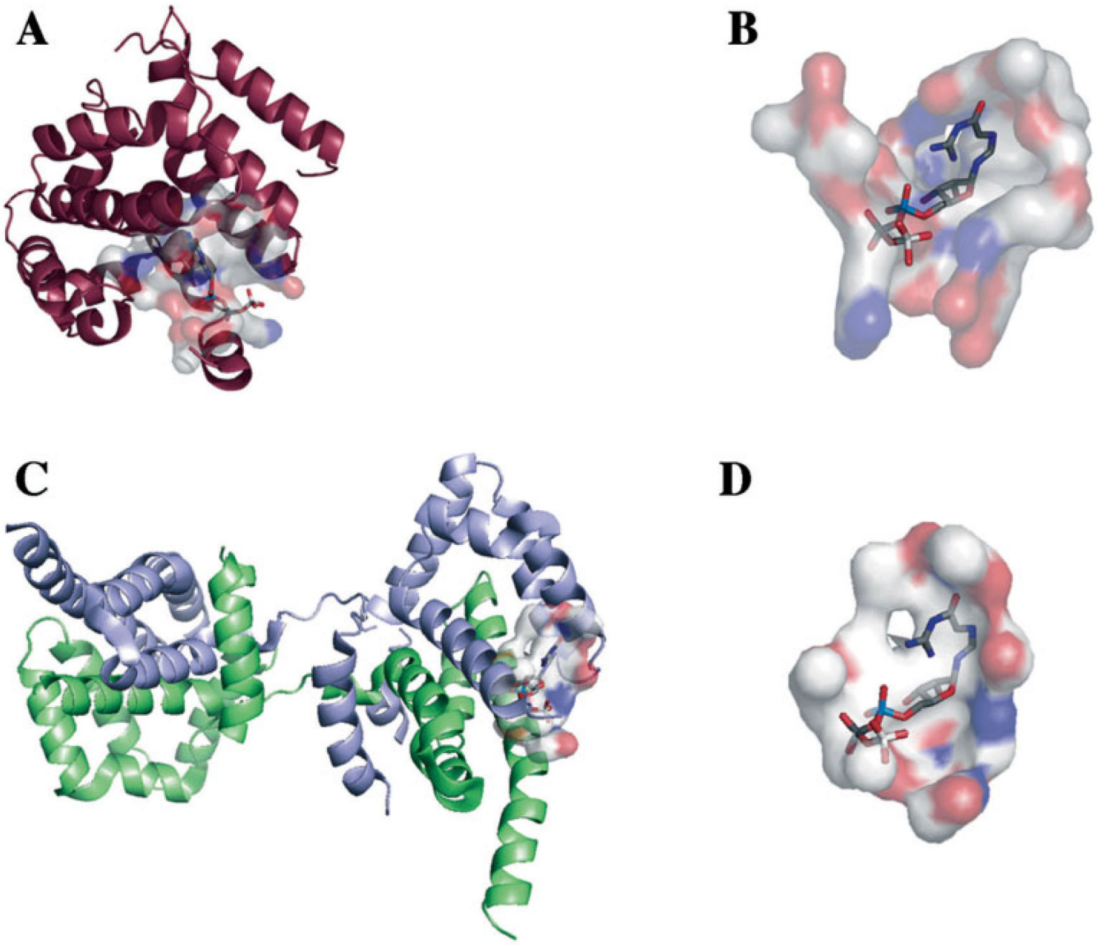

E

St-DmsD	R7A	D8A	D142A	E148A	E140A	F10A			I194A	L193A	L151A	C147A	T13A	
Sm-TorD	R10A	D197B		E48A		F51A	F41A		I6A	L45A				V13A
guanylyl cyclase	R976B	D929B	D885B	E925A	E1010B	F889B	F999A	F883A	I927A	L998A	L905B	C997A	T890B	V1003A

Figure 4.

Putative GTP binding sites for St-DmsD (**A**), Sm-TorD (**C**) are proposed based on similarity to a known GTP binding surface of guanylyl cyclase from H. sapiens (PDB code: 1AWL). A GTP molecule has been modeled into the corresponding surfaces (**B,D**) based on the superposition of conserved residues with chain identifiers following the residue numbers (**E**). Images prepared using the PyMol and the Global Protein Surface Survey plugin (http://gpss.mcsg.anl.gov).

Table I

Summary of Crystal MAD Data Collection

	Inflection	Peak
Wavelength (Å)	0.97913	0.97986
Resolution range (Å)	50.0-1.45 Å	50.0-1.38 Å
No. of unique reflections	86028 (6568)	93261 (5871)
Completeness (%)	93.9 (71.8)	91.6 (57.5)
Redundancy	4.4 (3.4)	4.6 (3.4)
R merge (%)	4.4 (38.0)	4.4 (41.2)

Data from the highest resolution shell are in the parentheses. Peak data were used for refinement. The resolution range for the highest shell is 1.44-1.38 Å with I/sigma 254.6/104.8.

Table II

Crystallographic Statistics

Resolution range (Å)	20-1.38 Å
No. of reflections (working set)	45922
No. of reflections (test set)	2481
Completeness for range (%)	96.5
σ Cutoff	none
R-value (%)	16.1
Free *R*-value (%)	18.5
Rms deviations from ideal geometry	
Bond length	0.013 Å
Angle	1.396°
No. of atoms	1953 in total
Protein	1654
Water	254
SO4	10
PEG 400	35
Mean *B* value ($Å^2$)	12.4
Ramanchandran plot statistics	
Residues in most favored regions	92.6%
Residues in allowed regions	7.4%
Residues in disallowed regions	0